Available online at www.sciencedirect.com

SciVerse ScienceDirect

Ceramics International 39 (2013) 6551–6558

CERAMICS INTERNATIONAL

www.elsevier.com/locate/ceramint

Temperature dependent magnetic properties of $CoFe_2O_4$/CTAB nanocomposite synthesized by sol–gel auto-combustion technique

U. Kurtan[a], R. Topkaya[b,*], A. Baykal[a], M.S. Toprak[c,d]

[a]Department of Chemistry, Fatih University, 34500 B.Çekmece-Istanbul, Turkey
[b]Department of Physics, Gebze Institute of Technology, 41400 Gebze-Kocaeli, Turkey
[c]Department of Materials and Nanophysics, KTH-Royal Institute of Technology, 16440 Kista-Stockholm, Sweden
[d]Department of Materials Science and Engineering, Yıldırım Beyazıt University, Ulus-Ankara, Turkey

Received 27 November 2012; received in revised form 11 January 2013; accepted 25 January 2013
Available online 4 February 2013

Abstract

A $CoFe_2O_4$/cetyl trimethylammonium bromide (CTAB) nanocomposite has been fabricated by a sol–gel auto-combustion method. Characterization of the material revealed the composition of the crystalline phase as $CoFe_2O_4$ while FT-IR confirmed the presence of CTAB on the nanoparticles. From X-ray line profile fitting, average crystallite size was estimated to be 22 ± 6 nm. SEM analysis showed a porous sheet-like morphology with internal nanosize grains of about 30 nm. The room temperature coercive field (H_c) of the $CoFe_2O_4$/CTAB nanocomposite was found to be 1045 Oe which is close to the previously reported room temperature values for bulk $CoFe_2O_4$. The H_c was observed to decrease almost linearly with the square root of the temperature ($\sqrt{T}$) according to *Kneller's law*. From the linear fit of H_c versus $\sqrt{T}$, the zero-temperature coercivity (H_{c0}) and superparamagnetic blocking temperature (T_B) of the $CoFe_2O_4$/CTAB nanocomposite were found to be ~9.1 kOe and ~425 K, respectively. The remanence magnetization (M_r), the reduced remanent magnetization (M_r/M_s), and the effective magnetic anisotropy (K_{eff}) decrease with increasing temperature. The M_r/M_s value of 0.6 at 10 K higher than the theoretical value of 0.5 for non-interacting single domain particles with the easy axis randomly oriented suggests the $CoFe_2O_4$/CTAB nanocomposite to have cubic magnetocrystalline anisotropy according to the Stoner–Wohlfarth model.

Keywords: Sol–gel; Auto-combustion; Ferromagnetic; $CoFe_2O_4$; Magnetic nanomaterials

1. Introduction

Spinel ferrites with nanosized dimensions have drawn considerable scientific and technological interests because of their applications in high-density magnetic recording media, magnetic fluids, catalysts, gas-sensor, high-performance electromagnetic and spintronic devices, etc. [1–4]. Most of these applications depend on the magnetic properties of the nanoparticles, such as superparamagnetism, spin-glass-like behavior, and spin canting effect, etc. The magnetic properties of the nanoparticles are substantially different from those of their bulk counterparts due to the large surface-to-volume ratio of these nanostructures. Among spinel ferrites, cobalt ferrite ($CoFe_2O_4$) is of particular interest because of its relatively high saturation magnetization, excellent chemical stability, mechanical hardness, and high cubic magneto-crystalline anisotropy [5].

It is well known that the magnetic properties of ferrite nanoparticles strongly depend on the particle size, chemical composition, shape of the nanoparticles, interactions between nanoparticles and especially preparation method. Several preparation techniques have been developed to synthesize $CoFe_2O_4$, such as co-precipitation [6], hydrothermal [7], dry and wet-milling [8], oxidation–reduction [9] and sol–gel auto-combustion method [10]. Among these preparation methods, the sol–gel auto-combustion method has recently attracted more interest because of the fact that it has the advantages of cheap precursors, simple preparation and a resulting ultrafine particles [11–13]. It is a unique

*Corresponding author. Tel.: +90 212 605 1319; fax: +90 212 653 8490.
E-mail addresses: rtopkaya@gyte.edu.tr, ramazantopkaya@yahoo.com (R. Topkaya).

0272-8842/$ - see front matter © 2013 Elsevier Ltd and Techna Group S.r.l. All rights reserved.
http://dx.doi.org/10.1016/j.ceramint.2013.01.088

combination of the combustion and the chemical gelation processes. This method has been used to control the size and morphology of nanoparticles determining the structural and magnetic properties. The process gives a homogeneous powder with a narrow size distribution and requires low energy [14]. Due to these advantages, the sol–gel auto-combustion method is vastly used to prepare the magnetic nanoparticles.

Numerous studies have been presented on the ferrite nanoparticles prepared by using the sol–gel auto-combustion method [15,16,17]. Kadam et al. have reported the synthesis of ultrafine crystal of $Li_{3x}MnFe_{2-x}O_4$ ferrite nanoparticles by sol–gel auto-combustion method [18]. Shirsath et al. observed the saturation magnetization value higher than bulk value for Dy^{3+} substituted Ni–Cu–Zn ferrite nanoparticles synthesized by the sol–gel auto-combustion method [19]. Cannas et al. have presented the structural properties of the ferrite (γ-Fe_2O_3 and $CoFe_2O_4$) and ferrite–silica composites with mean size of 3.5 and 5.0 nm [20]. Enhanced magnetic properties have been reported for $Zn_{1-x}Ni_xFe_2O_4$ ferrite nanoparticles prepared by sol–gel auto-combustion by Zhang et al. [21]. In virtue of these studies, it has been proved that the sol–gel auto-combustion method is a useful method to sythesize the ferrite nanoparticles.

The incorporation of nanoscaled inorganic particles and organic materials (such as polymers) has been widely investigated, considering the extra advantages that could be obtained with combined properties of the inorganic materials (mechanical strength, magnetic and thermal stability) and the organic polymers (flexibility, dielectric, ductility and processibility) [22]. It has been found that the CTAB surfactant prevents the agglomeration of the Fe_3O_4 nanoparticles by Zhu et al. [23].

In this present study, due to the many advantages mentioned above, the sol–gel auto-combustion method is applied for synthesizing the $CoFe_2O_4$/CTAB nanocomposite. The CTAB surfactant is used as a stabilizer to prevent the aggregation of particles. To the best of our knowledge, this is the first report in which the sol–gel auto-combustion method was used for the synthesis of $CoFe_2O_4$/CTAB nanocomposite. In this work, the magnetic properties of the $CoFe_2O_4$/CTAB nanocomposite synthesized by a sol–gel auto-combustion method have been investigated in details in the temperature range of 10–400 K and in magnetic fields up to 90 kOe.

2. Experimental

2.1. Chemicals and instrumentations

All chemicals including cobalt nitrate hexahydrate ($Co(NO_3)_2 \cdot 6H_2O$, iron nitrate nonahydrate $Fe(NO_3)_3 \cdot 9H_2O$, citric acid ($C_6H_8O_7$), cetyl trimethylammonium bromide ($C_{19}H_{42}NBr$) and ammonium hydroxide (NH_4OH) were obtained from Merck and used as received, without further purification.

X-ray powder diffraction (XRD) analysis was conducted on a Rigaku Smart Lab Diffractometer operated at 40 kV and 35 mA using Cu K_α radiation.

Scanning Electron Microscopy (SEM) analysis was performed, in order to investigate the microstructure of the sample, using FEI XL40 Sirion FEG Digital Scanning Microscope. Samples were coated with gold at 10 mA for 2 min prior to SEM analysis.

Fourier transform infrared (FT-IR) spectra were recorded in transmission mode (Perkin Elmer BX FT-IR) on powder samples that were ground with KBr and compressed into a pellet. FT-IR spectra in the range 4000–400 cm^{-1} were recorded in order to investigate the nature of the chemical bonds formed.

The thermal stability was determined by thermogravimetric analysis (TGA, Perkin Elmer Instruments model, STA 6000). The TGA thermograms were recorded for 5 mg of powder sample at a heating rate of 10 °C/min in the temperature range of 30–750 °C under nitrogen atmosphere.

The magnetization measurements were performed by using vibrating sample magnetometer (VSM, Quantum Design, PPMs 9T) in an external field up to 90 kOe in the temperature range of 10–400 K.

2.2. Synthesis

Stoichiometric amounts of cobalt nitrate hexahydrate ($Co(NO_3)_2 \cdot 6H_2O$) and iron nitrate nonahydrate ($Fe(NO_3)_2) \cdot 9H_2O$ powders in a molar ratio of Fe/Co = 2 were dissolved in deionized water. Equimolar quantity of citric acid to the total amount of metal ions was then added. The addition of citric acid helps the homogenous distribution and segregation of the metal ions [24–26]. The aqueous solution was neutralized by the addition of NH_4OH. The stoichiometric amount of *n*-cetyltrimethylammonium bromide surfactant ($C_{13}H_{30}BrN$) was dissolved in minimum amount of water then added to the above solution. The resultant solution was slowly evaporated at 100 °C until a gel (xerogel) formed. Continuous heating of xerogel leads to the formation of black nanopowder of nanocomposite through a self-propagating combustion process (150 °C).

3. Results and discussion

3.1. XRD analysis

The X-ray diffraction pattern of the final product is presented in Fig. 1 which indicates the presence of the spinel cubic structure [27] and the diffraction peaks are broadened owing to very small crystallite size. The mean size of the crystallites was estimated from the diffraction pattern by line profile fitting method using Eq. (1) given in Refs. [28,29]. The line profile, shown in Fig. 1, was fitted for observed seven peaks with the following miller indices: (111), (220), (311), (400), (422), (511) and (440) [30]. The average crystallite size was obtained as 22 ± 6 nm as a result of this line profile fitting.

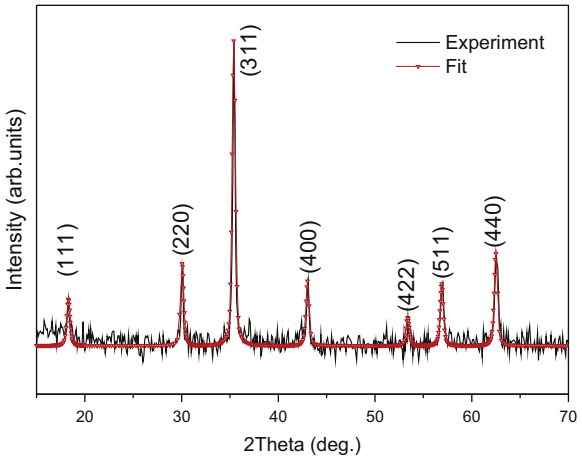

Fig. 1. X-ray powder diffraction pattern of $CoFe_2O_4$/CTAB nanocomposite.

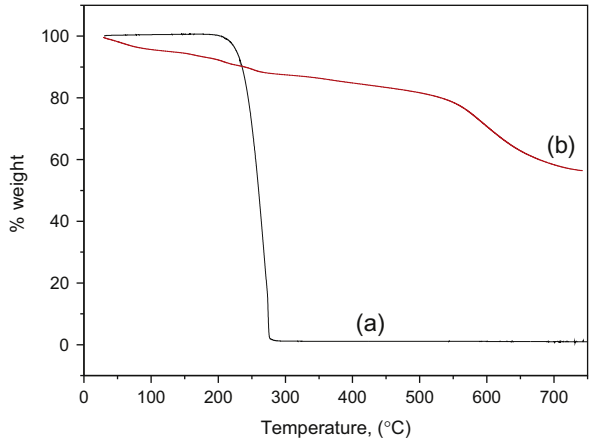

Fig. 3. TG thermograms of (a) CTAB and (b) $CoFe_2O_4$/CTAB nanocomposite.

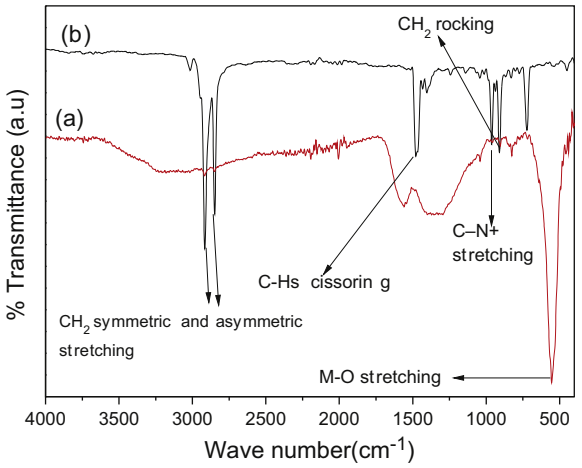

Fig. 2. FT-IR spectra of (a) CTAB and (b) $CoFe_2O_4$/CTAB nanocomposite.

3.2. FT-IR analysis

The FT-IR spectra of CTAB and $CoFe_2O_4$/CTAB nanocomposite are presented in Fig. 2a and b, respectively. Two main broad metal–oxygen bands are seen in the IR spectra of all spinels, and ferrites in particular. The highest one, v_1 (Fig. 2b) observed in the 603 cm^{-1}, corresponds to intrinsic stretching vibrations of the metal at the tetrahedral site, $M_{tetra} \leftrightarrow O$, whereas the v_2-lowest band, usually observed in the range 450–385 cm^{-1}, is assigned to octahedral-metal stretching, $M_{octa} \leftrightarrow O$ [31–33]. There is also some CTAB residue found in the product due to the low combustion temperature (ca. 150 °C). This is also confirmed by the presence of absorption peaks at 2918, 2855 and 1461 cm^{-1} in the spectrum. According to Dobson et al., two bands occurring at 2920 and 2855 cm^{-1} are due to the respective anti-symmetric and symmetric $–CH_2–$ vibrations of the carbon chains and the absorption band at 1465 cm^{-1} arises from the $–CH_2–$ bending or scissor mode of the CTAB tail [32,33].

3.3. TG analysis

To further investigate the structure of CTAB capped on the surface of $CoFe_2O_4$ NPs, TGA was conducted. Thermal behavior of both CTAB and the $CoFe_2O_4$/CTAB nanocomposite are given in Fig. 3a and b, respectively. In the case of CTAB (Fig. 3a), the weight loss occurred sharply from 220 to 320 °C, revealing that CTAB molecules were decomposed thermally within this temperature range. However, in the case of $CoFe_2O_4$/CTAB nanocomposite, the TGA curve shows two weight loss steps. The first weight loss step occurred sharply within ~220–500 °C (19% weight loss) and the second one gradually from ~500 to 700 °C (21% weight loss). Above 700 °C, thermal behavior of product is stable. These two weight loses in nanocomposite might be due to the CTAB and citric acid [34]. As it was observed from Fig. 3, the weight percentages of organic (CTAB) and inorganic layer ($CoFe_2O_4$) in nanocomposite were 40 and 60, respectively. By the help of TG analysis, the presence of CTAB on the surface of the $CoFe_2O_4$ NPs was also confirmed.

3.4. SEM analysis

Morphology and microstructure of fabricated nanocomposites are investigated by SEM and few micrographs are presented in Fig. 4. It is observed that the composite showed highly porous structure with thin sheet like morphology. The observed porosity is due to the evolution of gases during the decomposition process. These structures may have formed during the self-propagating reaction where the solvent evaporated very quickly, possibly remaining a viscous mixture of formed nanoparticles and the polymer forming these sheets. Close up views show the presence of very sharp faceted crystals as well as sheets with internal structure of about 30 nm grains.

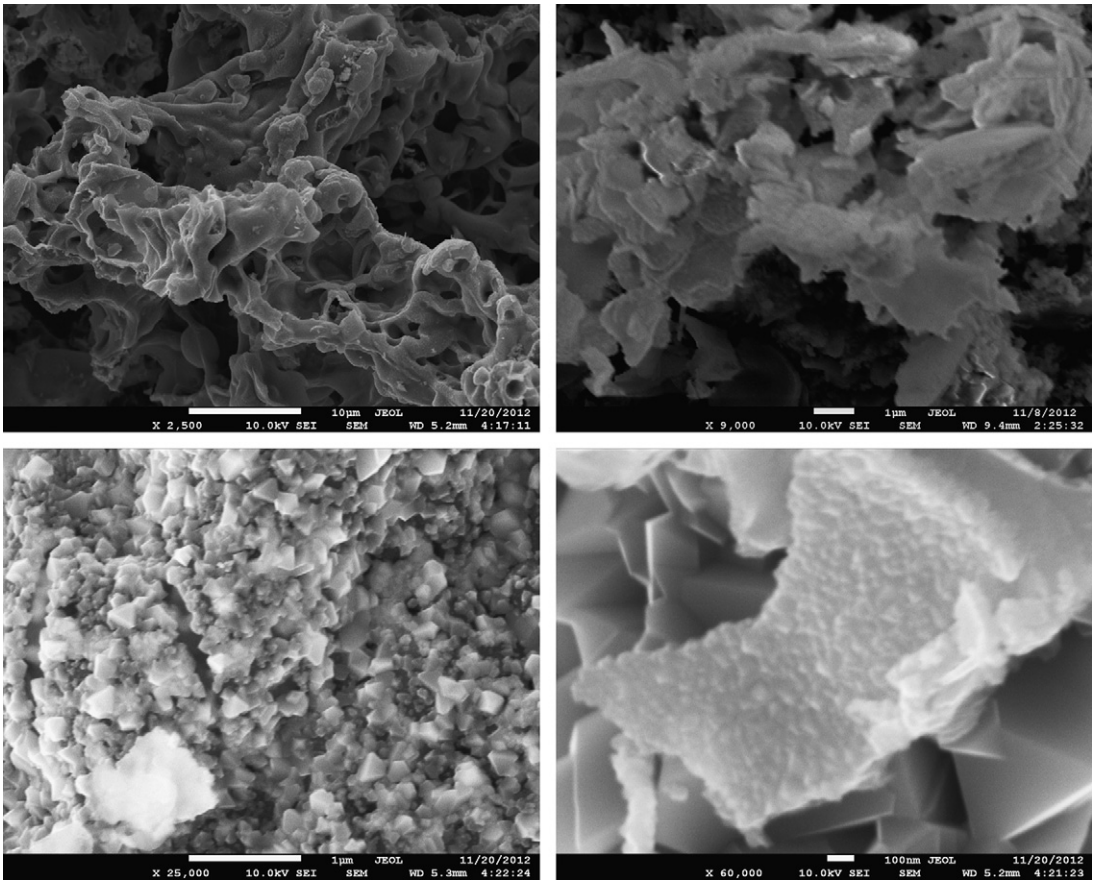

Fig. 4. SEM micrographs of $CoFe_2O_4$/CTAB nanocomposite.

3.5. VSM analysis

The magnetization curves as a function of the applied magnetic field at different temperatures are shown in Fig. 5 for the $CoFe_2O_4$/CTAB nanocomposite. The sample shows hysteretic behavior at all temperatures, indicating ferromagnetic behavior between 10 and 400 K. Comparing the M–H curves at different temperatures, the observed hysteretic behavior is reduced when the temperature is increased from 10 to 400 K. At the temperature of 400 K, a small hysteresis is still present, which suggests the blocking temperature of the sample prepared in this work is above 400 K. It is easily observed from Fig. 5 that at all temperatures, the magnetization does not reach saturation even at 90 kOe, which suggests the existence of antiferromagnetic interactions between ions [35,36]. Such behavior has been observed in the coated $Mn_xCo_{1-x}Fe_2O_4$ NPs prepared by the glycothermal reaction [36] and $Mn_{0.2}Ni_{0.8}Fe_2O_4$ NPs synthesized by a PEG-assisted hydrothermal route [37]. While the ferromagnetic contribution goes to the magnetization saturation, the antiferromagnetic contribution improves linearly the magnetization as the magnetic field increases, giving rise to a non-saturated magnetization.

The variation of the saturation magnetization (M_s) of the $CoFe_2O_4$/CTAB nanocomposite as a function of temperature is shown in Fig. 6. The M_s values at different temperatures were determined from the extrapolation of the M curve with $1/H$ as $1/H$ approaches zero. It can be easily seen that the M_s values of the $CoFe_2O_4$/CTAB nanocomposite decrease with increasing the temperature due to an increase of thermal fluctuations on magnetic ions with increasing the temperature and also are lower than that of bulk $CoFe_2O_4$ (80 emu/g) [38]. The lower magnetization values of nanoparticles are attributed to the surface spin disorder [39] or spin canting effect [40]. If the surface spins of the magnetic nanoparticle are not aligned with its magnetization direction, the magnetization value can be different from those of their bulk counterparts. Similar lower M_s values have been reported in nearly monodisperse $CoFe_2O_4$ NPs prepared under a simple hydrothermal condition [41], single domain $CoFe_2O_4$ nanoparticles synthesized by co-precipitating method [42] and $CoFe_2O_4$ nanofibers and nanoparticles fabricated using an electrospinning technique [43].

Fig. 7 shows the zero field cooled (ZFC) and field cooled (FC) curves of the $CoFe_2O_4$/CTAB nanocomposite measured in the temperature range of 10 and 400 K under applied magnetic field of 100 Oe. First, the sample was cooled down under zero external magnetic field and then the ZFC magnetization was recorded as the temperature rises from 10 to 400 K under an applied magnetic field of 100 Oe. Later, the sample was cooled down again under an applied field of

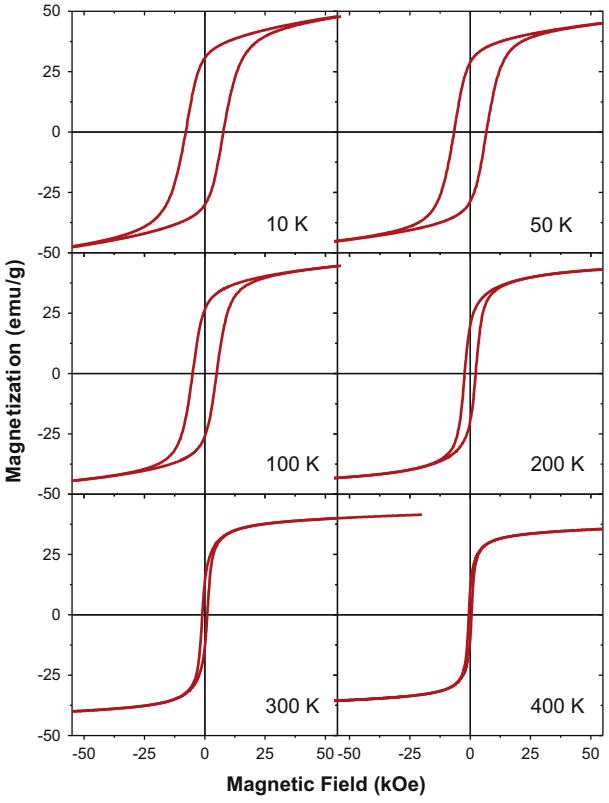

Fig. 5. Magnetic field dependence of the magnetization of $CoFe_2O_4$/CTAB nanocomposite at different temperatures.

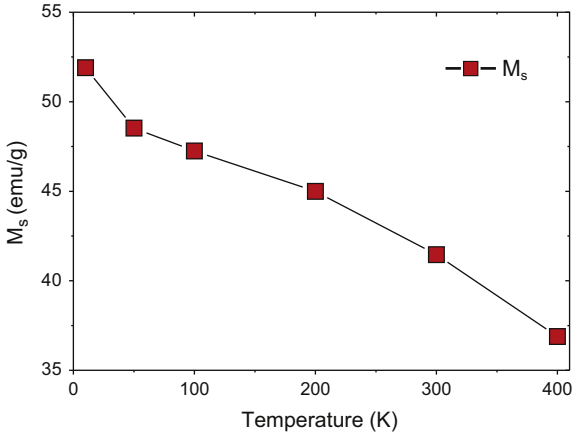

Fig. 6. Variation of saturation magnetization (M_s) of $CoFe_2O_4$/CTAB nanocomposite with temperature.

100 Oe and then the FC magnetization was recorded as the temperature rises from 10 to 400 K under an applied magnetic field of 100 Oe. As the temperature rises from 10 to 400 K, ZFC magnetization increases, however, it does not reach a maximum. In other words, the ZFC and FC measurement show an irreversible magnetic behavior below 400 K. This result means that the blocking temperature of the sample is above 400 K. Also, this result further confirms that the sample used in this study shows ferromagnetic behavior in the temperature range of 10–400 K.

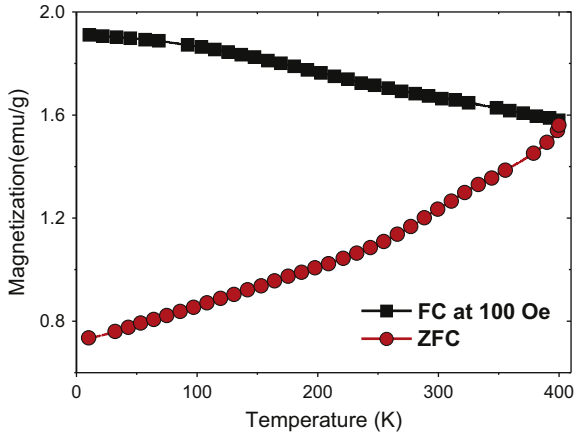

Fig. 7. Zero field cooled (ZFC) and field cooled (FC) curves for $CoFe_2O_4$/CTAB nanocomposite under an applied magnetic field of 100 Oe.

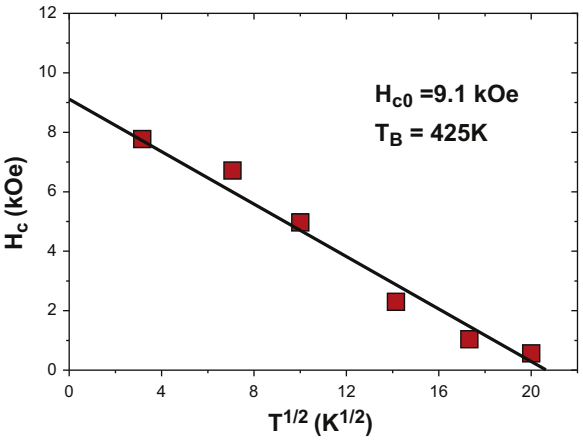

Fig. 8. $T^{1/2}$ dependence of coercive field (H_c) for the $CoFe_2O_4$/CTAB nanocomposite. Solid line shows the linear fit to the experimental data according to *Kneller's law*.

For non-interacting single domain magnetic particles with uniaxial anisotropy, the temperature dependence of coercivity in the temperature range of (0–T_B K) can be written as follows (*Kneller's law*) [44]:

$$H_c(T) = H_{c_0}\left[1-\left(\frac{T}{T_B}\right)^{1/2}\right] \quad (1)$$

where H_{c_0} is the coercive field at $T=0$ K and T_B is the superparamagnetic blocking temperature. Fig. 8 shows the $T^{1/2}$ dependence of the coercive field for the $CoFe_2O_4$/CTAB nanocomposite. The H_c of the $CoFe_2O_4$/CTAB nanocomposite decreases almost linearly with square root of the temperature and the data fit well to Kneller's relation (Eq. (1)) in the temperature range of 10–400 K, resulting in $H_{c_0} = \sim 9.1$ kOe and $T_B = \sim 425$ K.

In this work, the increase of the coercive field with decreasing temperature is due to the fact that the effective magnetic anisotropy increases with decreasing temperature. The H_c value of the $CoFe_2O_4$/CTAB nanocomposite used in this study is 1045 Oe at 300 K, which is very close

to the room temperature coercivity of bulk $CoFe_2O_4$ [45], but far from theoretical value calculated for a non-interacting single domain $CoFe_2O_4$ nanoparticles with cubic anisotropy.

The change in the remanence magnetization, M_r for the $CoFe_2O_4$/CTAB nanocomposite with temperature is plotted in Fig. 9. The inset in Fig. 9 shows thermal dependence of the reduced remanent magnetization (M_r/M_s) for the $CoFe_2O_4$/CTAB nanocomposite. It can be seen that the M_r and M_r/M_s almost linearly decrease with increasing temperature. This can be attributed to the decrease of magnetic anisotropy strength with increasing temperature [46,47]. According to the Stoner–Wohlfarth model, M_r/M_s for noninteracting single domain particles with the easy axis randomly oriented are given by $M_r/M_s=0.5$ for uniaxial anisotropy, and $M_r/M_s=0.832$ for cubic anisotropy [48]. As shown in the inset of Fig. 9, the M_r/M_s value of the sample used in this study is ~0.6 at 10 K, which is higher than theoretical value of 0.5. Considering that bulk $CoFe_2O_4$ has very high cubic magnetocrystalline anisotropy, it can be concluded that the $CoFe_2O_4$/CTAB nanocomposite used in this study have cubic magnetocrystalline anisotropy. Similar results have also been reported for nearly mono-dispersed $CoFe_2O_4$ nanoparticles synthesized by using the seed-mediated co-precipitation method [49] and single domain $CoFe_2O_4$ nanoparticles synthesized by co-precipitation method [42]. Also, in this case, the linear dependency of H_c on $T^{1/2}$ (Fig. 8) can be attributed to presence of ferromagnetically ordered single domain particles [50,51].

According to the Stoner–Wohlfarth model, the H_c for noninteracting single domain particles with the easy axis randomly oriented are given by $H_c=0.985\ K_{eff}/M_s$ for uniaxial anisotropy, and $H_c=0.64\ K_{eff}/M_s$ for cubic anisotropy [48]. It was understood from M_r/M_s results (Fig. 9) that the sample used in this study has cubic magnetocrystalline anisotropy. Thus, we used the relation $H_c=0.64\ K_{eff}/M_s$ to calculate the K_{eff}. Fig. 10 shows the

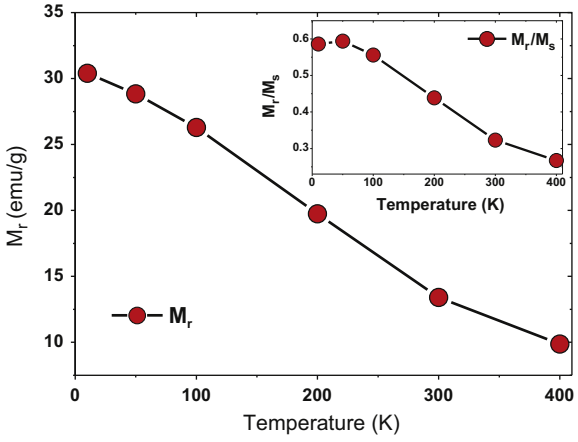

Fig. 9. Thermal dependence of the remanence magnetization, M_r for $CoFe_2O_4$/CTAB nanocomposite. Inset presents variation in the reduced remanent magnetization (M_r/M_s) with temperature.

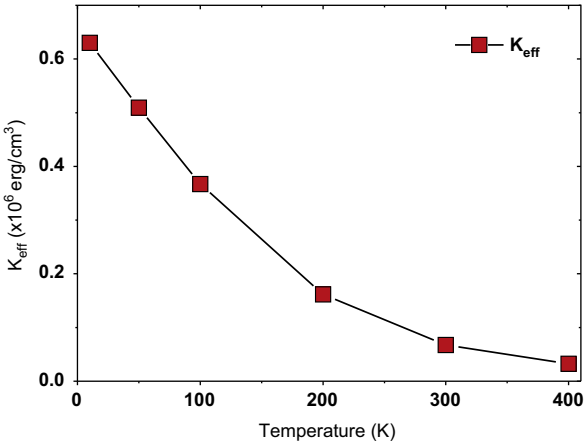

Fig. 10. Temperature dependence of effective magnetic anisotropy (K_{eff}) for $CoFe_2O_4$/CTAB nanocomposite.

dependence of effective magnetic anisotropy constant, K_{eff} on temperature. It is evident that the K_{eff} of the sample decreases with increasing temperature. The very high magnetocrystalline anisotropy of cobalt ferrite results from the existence of the Co^{2+} ions in the octahedral (B) sites of the spinel structure [52]. As temperature increases, the Co^{2+} ions migrate from octahedral (B) to tetrahedral (A) sites [53], and thus the K_{eff} decreases.

4. Conclusion

We presented a novel route for the fabrication of $CoFe_2O_4$/CTAB nanocomposite, which is based on a sol–gel auto-combustion method. Characterization of the fabricated material revealed the composition of the crystalline phase as $CoFe_2O_4$ while FT-IR confirmed the presence of CTAB on the $CoFe_2O_4$ nanoparticles. Average crystalite size was obtained as 22 ± 6 nm from X-ray line profile fitting. SEM analysis showed porous sheet-like morphology with internal nanosize grains of about 30 nm. It was found from magnetization measurements that the room teperature coercive field (H_c) value of the $CoFe_2O_4$/CTAB nanocomposite is 1045 Oe which is close to the room temperature coercivity of bulk $CoFe_2O_4$. From magnetization versus magnetic field measurements, it was found a linear dependence of the H_c for the $CoFe_2O_4$/CTAB nanocomposite as function of square root of the temperature ($\sqrt{T}$). From fitting the H_c values to *Kneller's law*, the coercive field at $T=0$ K and superparamagnetic blocking temperature (T_B) was determined as ~9.1 kOe and ~425 K, respectively. It was observed that the M_r, M_r/M_s and K_{eff} of the $CoFe_2O_4$/CTAB nanocomposite decrease with increasing temperature. The M_r/M_s values increase with decreasing temperature and reaches a maximum value of 0.6 at 10 K, indicates that the $CoFe_2O_4$/CTAB nanocomposite used in this work have cubic magnetocrystalline anisotropy according to the Stoner–Wohlfarth model.

Acknowledgments

This work is supported by Fatih University under BAP grant no P50021104-B and the State Planning Organization of Turkey (DPT-Project No. 2009K120730).

References

[1] Z. Zi, Y. Sun, X. Zhu, Z. Yang, J. Dai, W. Song, Synthesis and magnetic properties of $CoFe_2O_4$ ferrite nanoparticles, Journal of Magnetism and Magnetic Materials 321 (2009) 1251.
[2] J. Jiang, L.H. Ai, A.H. Liu, A novel poly(o-anisidine)/$CoFe_2O_4$ multifunctional nanocomposite: preparation, characterization and properties, Synthetic Metals 160 (2010) 333–336.
[3] L.J. Zhao, Q. Jiang, Solvothermal synthesis of Co/$CoFe_2O_4$ nanobelts, Materials Letters 64 (2010) 677–679.
[4] D.Y. Chen, Y.Y. Meng, D.C. Zeng, Z.W. Liu, H.Y. Yu, X.C. Zhong, CTAB-assisted low-temperature synthesis of $SrFe_{12}O_{19}$ ultrathin hexagonal platelets and its formation mechanism, Materials Letters 76 (2012) 84–86.
[5] L. Ai, J. Jiang, Influence of annealing temperature on the formation, microstructure and magnetic properties of spinel nanocrystalline cobalt ferrites, Current Applied Physics 10 (2010) 284.
[6] E. Karaoğlu, U. Özel, C. Caner, A. Baykal, M.M. Summak, H. Sözeri, Synthesis and characterization of $NiFe_2O_4$–Pd magnetically recyclable catalyst for hydrogenation reaction, Materials Research Bulletin 47 (2012) 4316–4321.
[7] E. Karaoğlu, T. Ozkaya, A. Baykal, Hydrothermal synthesis and characterization of PEG stabilized Co_3O_4 nanoparticles, Journal of Superconductivity and Novel Magnetism 25 (2012) 2403–2406.
[8] S. Ozcan, B. Kaynar, M.M. Can, T. Firat, Synthesis of $ZnFe_2O_4$ from metallic zinc and iron by wet-milling process, Materials Science and Engineering B 121 (3) (2005) 278–281.
[9] T. Ozkaya, A. Baykal, Y. Koseoğlu, H. Kavas, Synthesis of Co_3O_4 nanoparticles by oxidation-reduction method and its magnetic characterization, Central European Journal of Chemistry 7 (3) (2009) 410–414.
[10] G. Xu, H. Ma, M. Zhong, Influence of pH on characteristics of $BaFe_{12}O_{19}$ powder prepared by sol–gel auto-combustion, Journal of Magnetism and Magnetic Materials 301 (2) (2006) 383–388.
[11] J.F. Crider, Self-propagating high-temperature synthesis: a soviet method for producing ceramic materials, Ceramics Engineering and Science Proceedings 3 (1982) 519.
[12] M. Srivastava, S. Chaubey, K.O. Animesh, Investigation on size dependent structural and magnetic behavior of nickel ferrite nanoparticles prepared by sol–gel and hydrothermal methods, Materials Chemistry and Physics 118 (1) (2009) 174–180.
[13] S.S. Madani, G. Mahmoudzadeh, S.A. Khorrami, Influence of pH on the characteristics of cobalt ferrite powder prepared by a combination of sol–gel auto-combustion and ultrasonic irradiation techniques, Journal of Ceramic Processing Research 13 (2) (2012) 123–126.
[14] S.A. Khorrami, G. Mahmoudzadeh, S.S. Madani, F. Gharib, Effect of calcination temperature on the particle sizes of zinc ferrite prepared by a combination of sol–gel auto combustion and ultrasonic irradiation techniques, Journal of Ceramic Processing Research 12 (5) (2011) 504–508.
[15] T. Slatineanu, E. Diana, V. Nica, V. Oancea, O.F. Caltun, A.R. Iordan, M.N. Palamaru, The influence of the chelating/combustion agents on the structure and magnetic properties of zinc ferrite, Central European Journal of Chemistry 10 (6) (2012) 1799–1807.
[16] K.H. Wu, Y.C. Chang, G.P. Wang, Preparation of NiZn ferrite/SiO_2 nanocomposite powders by sol–gel auto-combustion method, Journal of Magnetism and Magnetic Materials 269 (2004) 150–155.
[17] A. Sutka, K.A. Gross, G. Mezinskis, G. Bebris, M. Knite, The effect of heating conditions on the properties of nano- and microstructured Ni–Zn ferrite, Physica Scripta 83 (2011) 025601.
[18] R.H. Kadam, A.R. Biradar, M.L. Mane, S.E. Shirsath, Sol–gel auto-combustion synthesis of $Li_{3x}MnFe_{2-x}O_4$ and their characterizations, Journal of Applied Physics 112 (2012) 043902.
[19] S.E. Shirsath, R.H. Kadam, S.M. Patange, M.L. Mane, A. Ghasemi, A. Morisako, Enhanced magnetic properties of Dy^{3+} substituted Ni—Cu—Zn ferrite nanoparticles, Applied Physics Letters 100 (2012) 042407.
[20] C. Cannas, A. Musinu, D. Peddis, G. Piccaluga, New synthesis of ferrite–silica nanocomposites by a sol–gel auto-combustion, Journal of Nanoparticle Research 6 (2004) 223–232.
[21] H.E. Zhang, B.F. Zhang, G.F. Wang, X.H. Dong, Y. Gao, The structure and magnetic properties of $Zn_{1-x}Ni_xFe_2O_4$ ferrite nanoparticles prepared by sol–gel auto-combustion, Journal of Magnetism and Magnetic Materials 312 (2007) 126–130.
[22] H. Sugimoto, K. Daimatsu, E. Nakanishi, Y. Ogasawara, T. Yasumura, K. Inomata, Preparation and properties of poly (methylmethacrylate)–silica hybrid materials incorporating reactive silica nanoparticles, Polymer 47 (2006) 3754–3759.
[23] H. Guo, H. Zhu, H. Lin, J. Zhang, Polyaniline/Fe_3O_4 nanocomposites synthesized under the direction of cationic surfactant, Materials Letters 62 (2008) 2196.
[24] A. Pradeep, P. Priyadharsini, G. Chandrasekaran, Production of single phase nano size $NiFe_2O_4$ particles using sol–gel auto combustion route by optimizing the preparation conditions, Materials Chemistry and Physics 112 (2008) 572.
[25] P. Sivakumar, R. Ramesh, A. Ramanand, S. Ponnusamy, C. MuthamizHchelvan, Synthesis, studies and growth mechanism of ferromagnetic $NiFe_2O_4$ nanosheet, Applied Surface Science 258 (2012) 6648–6652.
[26] J. Azadmanjiri, S.A. Seyyed Ebrahimi, Influence of stoichiometry and calcination condition on the microstructure and phase constitution of $NiFe_2O_4$ powders prepared by sol–gel autocombustion method, Physica Status Solidi (c) 1 (2004) 3414.
[27] H. Liu, F. Xu, L. Li, Y. Wang, H. Qiu, A novel $CoFe_2O_4$/polyacrylate nanocomposite prepared via an in situ polymerization in emulsion system, Reactive and Functional Polymers 69 (2009) 43–47.
[28] T. Wejrzanowski, R. Pielaszek, A. Opalinska, H. Matysiak, W. Łojkowski, K.J. Kurzydłowski, Quantitative methods for nanopowders characterization, Applied Surface Science 253 (2006) 204.
[29] R. Pielaszek, Analytical expression for diffraction line profile for polydispersive powders, in: Applied Crystallography, Proceedings of the XIX Conference, Krakow, Poland, 2003, pp. 43.
[30] N. Kasapoğlu, A. Baykal, Y. Köseoğlu, M.S. Toprak, Microwave-assisted combustion synthesis of $CoFe_2O_4$ with urea, and its magnetic characterization, Scripta Materialia 57 (2007) 441.
[31] F. Gözüak, Y. Köseoğlu, A. Baykal, H. Kavas, Synthesis and characterization of $Co_xZn_{1-x}Fe_2O_4$ magnetic nanoparticles via a PEG-assisted route, Journal of Magnetism and Magnetic Materials 321 (2009) 2170.
[32] K.D. Dobson, A.D.R. Lanzilotta, A.J. McQuillan, An in situ infrared spectroscopic investigation of adsorption of sodium dodecylsulfate and of cetyltrimethylammonium bromide surfactants to TiO_2, ZrO_2, Al_2O_3, and Ta_2O_5 particle films from aqueous solutions, Vibrational Spectroscopy 24 (2000) 287.
[33] A. Baykal, N. Kasapoğlu, Y. Köseoğlu, M.S. Toprak, H. Bayrakdar, CTAB-assisted hydrothermal synthesis of $NiFe_2O_4$ and its magnetic characterization, Journal of Alloy Compounds 464 (2008) 514.
[34] M.R. Barati, S.A.S. Ebrahimi, A. Badiei, The role of surfactant in synthesis of magnetic nanocrystalline powder of $NiFe_2O_4$ by sol–gel auto-combustion method, Journal of Non-Crystalline Solids 354 (2008) 5184–5185.
[35] K.K. Bharathi, R.J. Tackett, C.E. Botez, C.V. Ramana, Coexistence of spin glass behavior and long-range ferrimagnetic ordering in La- and Dy-doped Co ferrite, Journal of Applied Physics 109 (2011) 07A510.
[36] R. Topkaya, Ö. Akman, S. Kazan, B. Aktaş, Z. Durmus, A. Baykal, Surface spin disorder and spin-glass-like behavior in manganese-

substituted cobalt ferrite nanoparticles, Journal of Nanoparticle Research 14 (2012) 1156.
[37] Y. Köseoğlu, M. Bay, M. Tan, A. Baykal, H. Sözeri, R. Topkaya, N. Akdoğan, Magnetic and dielectric properties of $Mn_{0.2}Ni_{0.8}Fe_2O_4$ nanoparticles synthesized by PEG-assisted hydrothermal method, Journal of Nanoparticle Research 13 (2011) 2235–2244.
[38] B.D. Cullity, Introduction to Magnetic Materials, 2nd edn., Addison-Wesley, New Jersey, 2009, p. 227.
[39] R.H. Kodama, A.E. Berkowitz, E.J. McNiff Jr, S. Foner, Surface spin disorder in $NiFe_2O_4$ nanoparticles, Physical Review Letters 77 (1996) 394–397.
[40] J.M.D. Coey, Noncollinear spin arrangement in ultrafine ferrimagnetic crystallites, Physical Review Letters 27 (1971) 1140–1142.
[41] X.H. Li, C.L. Xu, X.H. Han, L. Qiao, T. Wang, F.S. Li, Synthesis and magnetic properties of nearly monodisperse $CoFe_2O_4$ nanoparticles through a simple hydrothermal condition, Nanoscale Research Letters 5 (2010) 1039–1044.
[42] D. Pal, M. Mandal, A. Chaudhuri, B. Das, D. Sarkar, K. Mandal, Micelles induced high coercivity in single domain cobalt-ferrite nanoparticles, Journal of Applied Physics 108 (2010) 124317.
[43] M. Sangmanee, S. Maensiri, Nanostructures and magnetic properties of cobalt ferrite ($CoFe_2O_4$) fabricated by electrospinning, Applied Physics A (2009) 167–177.
[44] E.F. Kneller, F.E. Luborsky, Particle size dependence of coercivity and remanence of single-domain particles, Journal of Applied Physics 34 (1963) 656.
[45] D.J. Craik, Magnetic Oxides, Part 2, John Wiley & Sons, London, 1975, pp. 703.
[46] N.D. Chaudhari, R.C. Kambale, D.N. Bhosale, S.S. Suryavanshi, S.R. Sawant, Thermal hysteresis and domain states in Ni–Zn ferrites synthesized by oxalate precursor method, Journal of Magnetism and Magnetic Materials 322 (2010) 1999–2005.
[47] J.H. Fendler, Nanoparticles and Nanostructured Films, Wiley-VCH, 1998, pp. 81.
[48] E.C. Stoner, E.P. Wohlfarth, A mechanism of magnetic hysteresis in heterogeneous alloys, Philosophical Transactions of The Royal Society of London Series A 240 (1948) 599–642.
[49] C.N. Chinnasamy, B. Jeyadevan, K. Shinoda, K. Tohji, D.J. Djayaprawira, M. Takahashi, R. Justin Joseyphus, A. Narayanasamy, Unusually high coercivity and critical single-domain size of nearly monodispersed $CoFe_2O_4$ nanoparticles, Applied Physics Letters 83 (2003) 2862.
[50] S. Mitra, K. Mandal, P.A. Kumar, Temperature dependence of magnetic properties of $NiFe_2O_4$ nanoparticles embeded in SiO_2 matrix, Journal of Magnetism and Magnetic Materials 306 (2006) 254.
[51] X. Batlle, M. Garcia del Muro, J. Tejada, H. Pfeiffer, G.E. Sinn, Magnetic study of *M*-type doped barium ferrite nanocrystalline powders, Journal of Applied Physics 74 (1993) 3333.
[52] M. Tachiki, Origin of the magnetic anisotropy energy of cobalt ferrite, Progress Theoretical Physics 23 (1960) 1055–1072.
[53] A. Franco, F.C. Silva Jr, High temperature magnetic properties of cobalt ferrite nanoparticles, Applied Physics Letters 96 (2010) 172505.